



**HAL**  
open science

## Graphene saturable absorber mirror for passive mode-locking of mid-infrared QCLs

A. Outafat, S. Faci, Stéphane Protat, Elodie Richalot, Catherine Algani

► **To cite this version:**

A. Outafat, S. Faci, Stéphane Protat, Elodie Richalot, Catherine Algani. Graphene saturable absorber mirror for passive mode-locking of mid-infrared QCLs. *Optical and Quantum Electronics*, 2022, 54 (12), pp.850. 10.1007/s11082-022-04230-5 . hal-04040242

**HAL Id: hal-04040242**

**<https://hal.science/hal-04040242>**

Submitted on 31 Jan 2024

**HAL** is a multi-disciplinary open access archive for the deposit and dissemination of scientific research documents, whether they are published or not. The documents may come from teaching and research institutions in France or abroad, or from public or private research centers.

L'archive ouverte pluridisciplinaire **HAL**, est destinée au dépôt et à la diffusion de documents scientifiques de niveau recherche, publiés ou non, émanant des établissements d'enseignement et de recherche français ou étrangers, des laboratoires publics ou privés.

# Graphene Saturable Absorber Mirror for Passive Mode-locking of Mid-Infrared QCLs

Amine Outafat, Salim Faci, *Senior Member, IEEE*, Stéphane Protat, Elodie Richalot, *Member, IEEE* and Catherine Algani

**Abstract**—Passive mode-locking in quantum cascade lasers (QCLs) remains one of the huge challenges because of the fast relaxation time of the excited carriers which is typically in the range of sub-picoseconds. The use of conventional techniques such as the semiconductor saturable absorber mirror is inefficient because the spatial hole burning effect dominates the carrier dynamics. To overcome this effect, longitudinal transition structures with relaxation time around 50 ps were proposed. However, mode-locking is assured with an external modulation at a cavity roundtrip frequency. In this paper, we demonstrate that a single-layer graphene used as a saturable absorber permits to generate stable pulses in such structures. The graphene is integrated with a highly reflective mirror to increase the internal electric field and achieve the saturation intensity. The dynamic of the QCL is modeled with Maxwell-Bloch equations and the graphene layer with Maxwell-Ampere equation. This system of equations is solved using the one-dimensional Finite-Difference Time-Domain (FDTD) method. To model the graphene layer of 0.33 nm thickness, a specific sub-cell is implemented using Maloney method. Simulation results show a generation of isolated pulses with a peak electric field of  $80 \frac{MV}{m}$  and a duration of 51 fs. The mode-locking remains stable for the QCL with a vertical transition having a relaxation time below 5 ps.

**Index Terms**—Quantum Cascade Laser, Mode-locked laser, Maxwell-Bloch equations, Graphene, Numerical simulation, FDTD.

## I. INTRODUCTION

QUANTUM cascade lasers (QCL) have energy transitions located either in the conduction band or in the valence band. These transitions are obtained by engineering of quantum well structures and permit the generation of photons in mid- and far-infrared regions or in THz region [1], [2]. The performances of QCLs have been greatly enhanced and devices are today commercially available. QCLs have become one of the most important compact light sources in the mid-infrared region (MIR). However, the mode-locking of QCLs for the generation of ultrashort pulses remains one of the targeted challenge because of the fast gain recovery time compared to the roundtrip time of a  $\sim 3$  mm cavity length. In mode-locking theory, the phase lock of the laser longitudinal modes is obtained by a modulation of losses with a period equal to the cavity roundtrip time. This modulation can be driven externally with a sinusoidal signal or passively from the intensity-dependent loss mechanism induced by the

pulse energy. The active mode-locking of MIR QCLs is only obtained for a current injection close to the threshold. When the laser operates at higher current injection, spatial hole burning (SHB) effect governs the laser dynamic which induces instability in the mode-locking [3], [4]. In [5], we have proposed to integrate a single-layer graphene to one of the facets of the QCL structure to improve the active mode-locking. This leads to higher current injection increasing thus the pulse intensities and at the same time decreasing the pulse width. However, it is more difficult to achieve passive mode-locking in a monolithic two-section cavity because it requires specific absorbing conditions. Talukder and Menyuk [6] gave the conditions of such two-section cavity where one section provides gain while the other one induces quantum coherent absorption acting as a saturable absorber. The disadvantage of this structure is that the ratio of dipole moments of the absorber to the gain medium must be greater than two, which makes the monolithic solution impractical. Another solution is the interleaving of absorption and gain periods where the self-induced transparency (SIT) effect is exploited [7]. SIT mode-locked QCLs can produce stable pulses of the order of  $\sim 100$  fs duration over a broad parameter range.

In this work, we investigate the passive mode-locking of MIR QCLs by using graphene as saturable absorber. For such laser with ultrashort gain recovery time, fast saturable absorber is required. The relaxation time of graphene is very fast compared the gain recovery time and also to the pulse width making this solution efficient for QCL mode-locking. In addition, the saturation intensity in graphene is very low compared to the saturation intensity in semiconductor saturable absorber mirrors (SESAM). Single-layer graphene exhibits an absorbance ( $\alpha\pi = 2.3\%$ ) [8] which is 50 times higher than the absorbance of GaAs with the same thickness [9]. This means that graphene can be easily saturated due to the high optical absorption. The use of fast saturable absorber effect of graphene have been investigated in mode-locking of lasers. In [10], the graphene was used in the cavity of a fiber laser demonstrating a slight improvement. In semiconductor laser, the graphene has also been used as a saturable absorber for mode-locking of a  $1.55 \mu\text{m}$  semiconductor laser diode [11]. Recently, Mezzapesa *et al.* [12] have been demonstrated the integration of graphene in THz QCL frequency comb.

The laser dynamic is modeled here using Maxwell-Bloch equations in two atom-level approximation. The resolution of these equations is performed using one-dimensional Finite-Difference Time-Domain (FDTD) method. The graphene layer has a thickness of one carbon atom [13] and the distance

Amine Outafat, Salim Faci and Catherine Algani are with Univ Gustave Eiffel, CNAM, CNRS, ESYCOM, 292 Rue Saint-Martin, 75003 Paris.

Elodie Richalot and Stéphane Protat are with Univ Gustave Eiffel, CNRS, ESYCOM, F-77454 Marne-la-Vallée, France

Manuscript received July, 2022.

between two graphene layers is estimated to 0.33 nm [14]. The modeling of the graphene as a single FDTD-cell requires the discretization of the space as thin as its width which could have a negative impact on the computation time. To deal with this issue, the graphene layer can be considered in a cell of larger size but with an effective value of the nonlinear conductivity [11], [12]. We adopted such approach in our previous work [5] where two different methods have been used to model the nonlinear interaction of the light-wave with the graphene layer. In this paper, the single-layer graphene is modeled using a specific method suitable for thin layers in FDTD method [16]. In this method, the graphene is localized in a sub-cell completed with  $SiO_2$  material. The dielectric constant and the nonlinear conductivity of the graphene is calculated according to the method specifications.

The remaining of the paper is organized as follows: in section II, the Maxwell-Bloch equations for QCL and the Maxwell's equations for graphene are briefly described. In section III, the implementation of the FDTD method to solve the QCL and graphene equations is presented. Section IV describes the simulation results of a passive mode-locked QCL integrating a single-layer graphene. The last section gives a general conclusion of this work.

## II. STRUCTURE MODELING

### A. Structure description

Fig. 1 describes the total structure where the graphene is inserted between the QCL gain medium and the Bragg mirror. The Bragg mirror is composed of 7 layers grating of a high refractive index  $PbSe$  and a low refractive index  $BaF_2$ . The thickness of each layer is equal to a quarter of the propagating wavelength in the related medium. The total length of the laser cavity is 2.6 mm. The combination of the graphene and the high reflective mirror forms what is called graphene saturable absorber mirror. A  $SiO_2$  layer is added between the graphene and Bragg mirror to control the overlap between the absorbing layer and the maximum field intensity. This filed intensity profile is due to the interference between incident and reflected light-waves from the mirror. At the optimized graphene location, the intensity of the electric field can increase up to 400% allowing to reach the saturation intensity [17].

### B. Quantum cascade laser modeling

The QCL dynamics are modeled following the open two-level atom approximation following Maxwell-Bloch equations [18]. This model describes the interaction of ultrashort pulse light with a nonlinear medium which couple Maxwell's equations (1a)-(1b) and Bloch equations (1c)-(1e).

$$\frac{\partial H}{\partial t} = -\frac{1}{\mu_0} \frac{\partial E}{\partial y} \quad (1a)$$

$$\frac{\partial E}{\partial t} = -\frac{1}{\varepsilon_0 \varepsilon_r} \frac{\partial H}{\partial y} - \frac{N\mu}{\varepsilon_0 \varepsilon_r T_2} \rho_a + \frac{N\mu \omega_0}{\varepsilon_0 \varepsilon_r} \rho_b - l_0 E \quad (1b)$$

$$\frac{\partial \rho_a}{\partial t} = \omega_0 \rho_b - \frac{1}{T_2} \rho_a \quad (1c)$$

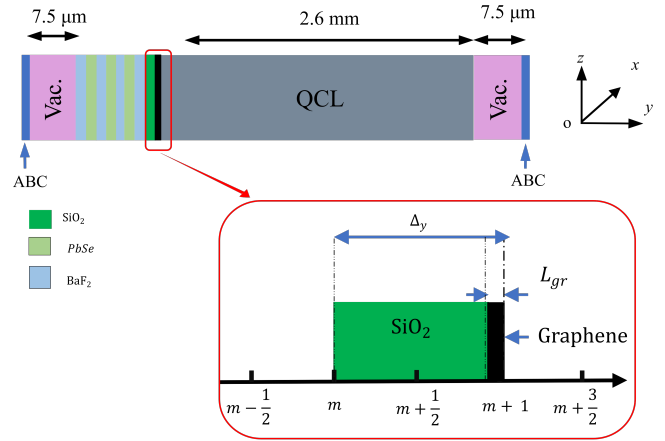


Fig. 1. Structure of the QCL with graphene based mirror.

$$\frac{\partial \rho_b}{\partial t} = -\omega_0 \rho_a - \frac{1}{T_2} \rho_b + \frac{2\mu E}{\hbar} \Delta \quad (1d)$$

$$\frac{\partial \Delta}{\partial t} = -\frac{2\mu E}{\hbar} \rho_b - \frac{\Delta}{T_1} + I + D \frac{\partial^2 \Delta}{\partial y^2} \quad (1e)$$

where  $E$  is the electric field along  $z$ -axis,  $H$  is the magnetic field along  $x$ -axis,  $l_0$  is the linear loss per unit length,  $\varepsilon_0$  is the dielectric constant of vacuum,  $\varepsilon_r$  is the relative permittivity,  $\mu_0$  is the vacuum permeability,  $\rho_a$  and  $\rho_b$  are the existence probability of electron in state  $a$  and  $b$  respectively, with  $a$  and  $b$  referring respectively to the ground and excited states,  $\mu$  is the electric dipole moment of a two-energy level atom,  $\Delta$  is the inversion population,  $T_1$  is the excited-state lifetime and  $T_2$  the coherence time,  $\hbar$  is the reduced Planck constant,  $\omega_0$  is the transition frequency. The overlap factor between the laser mode and the active region is chosen equal to unity.

These equations are solved using 1D-FDTD method along a propagation following  $y$ -axis. The mirror reflections modeled through Fresnel reflection coefficients induce the growth of standing waves inside the cavity.

### C. Single-layer graphene modeling

The physical parameter of the single-layer graphene involved here is the saturable absorption. To consider this nonlinear behavior, the graphene can be modeled in different ways. In [11], two-level rate equations have been considered for the semiconductor laser (gain medium) and the graphene layer (absorbing medium) coupled to Maxwell's equations. The dynamic of the carrier density has been described using the electric conductivity that is calculated from the saturable absorption coefficient following the equation (4). In [12], the Maxwell-Bloch equations integrating the saturable absorption have been discussed by describing the saturable absorbers as an open two-level system. The dipole moment and charge carrier density values have been determined from the saturation intensity and saturable absorption coefficient, respectively. Here, we model the graphene using the Maxwell-Ampere equation by determining the nonlinear conductivity from the graphene saturable absorption. We have compared

such approach with Maxwell-Bloch equations in [5] and close results have been obtained with the two methods.

To model the graphene conductivity from the electromagnetic wave absorption coefficient, the general expression (2) is used [19].

$$\sigma = \varepsilon_0 \varepsilon_r \omega \sqrt{\left[ \left( \frac{\sqrt{2} c}{\omega n_g} \alpha \right)^2 + 1 \right]^2 - 1} \quad (2)$$

where  $c$  is light velocity,  $n_g$  is the refractive index and  $\alpha$  is the absorption coefficient.

In the frequency range of the mid-infrared region, the condition  $\left( \frac{\sigma}{\varepsilon_0 \varepsilon_r \omega} \right)^2 \ll 1$  applies and the below approximation may be used

$$\sigma(I) \approx \frac{2 n}{\eta_0} \alpha(I) \quad (3)$$

with  $\eta_0$  the vacuum wave impedance.

The absorption coefficient of graphene depends on the light intensity following

$$\alpha(I) = \frac{\alpha_s}{1 + \frac{I}{I_{sat}}} + \alpha_{ns} \quad (4)$$

where  $\alpha_s$  is the saturable absorption and  $\alpha_{ns}$  is the non-saturable absorption estimated experimentally with the z-scan technique to respectively 0.72 and 0.13 [15].  $I = \frac{n}{\eta_0} |E|^2$  is the field intensity and  $I_s = \frac{n_g}{\eta_0} |E_s|^2$  is the field saturation intensity of graphene estimated to be 0.2 MW.cm<sup>-2</sup> at 10  $\mu$ m wavelength [20].

Thus, the system of equations that describes the interaction of electromagnetic field with graphene is as follows

$$\frac{\partial H}{\partial t} = -\frac{1}{\mu_0} \frac{\partial E}{\partial y} \quad (5a)$$

$$\frac{\partial E}{\partial t} = -\frac{1}{\varepsilon_0 \varepsilon_{rg}} \frac{\partial H}{\partial z} - \frac{\sigma(I)}{\varepsilon_0 \varepsilon_{rg}} E \quad (5b)$$

with  $\varepsilon_{rg}$  the real permittivity of graphene.

From (3) and (5b), the Maxwell-Ampere equation becomes

$$\frac{\partial E}{\partial t} = -\frac{1}{\varepsilon_0 \varepsilon_{rg}} \frac{\partial H}{\partial z} - \frac{2 n_g}{\varepsilon_0 \varepsilon_{rg} \eta_0} \left( \alpha_{ns} + \frac{\alpha_s}{1 + \left| \frac{E}{E_s} \right|^2} \right) E \quad (6)$$

In our previous work [5], the single-layer graphene has been modeled by one cell of FDTD grids. The nonlinear conductivity has been determined from the normalized absorption coefficient considering a cell spatial step of 31nm. However, we use here the realistic thickness of single-layer graphene which is typically 0.33 nm. The FDTD cell size cannot be chosen at such a small value because the structure dimension is much larger and the time step  $\Delta t$  would be very short. Then, a specific method proposed in [16] is used. The graphene is located in a thin part of the FDTD cell and the rest of the cell is completed with another material (see Fig. 1). We chose the  $SiO_2$  material to complete the cell size. The implementation

of this method requires a new conductivity  $\sigma_M$  and a dielectric constant  $\varepsilon_M$  of the considered cell as following

$$\sigma_M(I) = d \sigma(I) \quad (7a)$$

$$\varepsilon_M = (1 - d) \varepsilon_0 \varepsilon_{SiO_2} + d \varepsilon_0 \varepsilon_{rg} \quad (7b)$$

where  $d = \frac{L_g}{\Delta y}$  is the ratio between the graphene thickness ( $L_g$ ) and the cell size ( $\Delta y$ ), and  $\varepsilon_{SiO_2}$  is the  $SiO_2$  relative dielectric constant.

From these new defined parameters, we can rewrite equation (6) as

$$\frac{\partial E}{\partial t} = \frac{1}{\varepsilon_M} \frac{\partial H}{\partial z} - \frac{2d n_g}{\varepsilon_M \eta_0} \left[ \alpha_{ns} + \alpha_s \left( 1 + \frac{E}{E_s} \right)^{-2} \right] E \quad (8)$$

### III. NUMERICAL IMPLEMENTATION

The differential equations are solved using the finite-difference time-domain method. This method was proposed by Yee in 1966 [21] to solve complex RF-structures and was generalized to photonic structures and light/matter dynamic interaction analyses [22]. More recently, the FDTD was used to simulate the passive mode-locking of semiconductor diode laser [11] and THz frequency comb QCL [12] based on graphene as saturable absorber. As FDTD involves the discretization of time and space to form cells, its application to solve equations (1a)-(1e) is not trivial because of the mutual parameters dependence. Specially, the expression (1b) includes variables computed at the same time steps. This description is an explicit scheme which requires additional numerical methods. A complete nonlinear model for wave propagation in a two-level atom system has been demonstrated in [18] using an FDTD with an iterative predictor-corrector method to solve the Maxwell-Bloch equations. This model is able to predict saturation effects as well as self-induced transparency.

#### A. Quantum cascade laser

In order to keep the formulation explicit, the weak coupling approach is used to solve the system of QCL equations. The Maxwell-Ampere equation (1b) and Bloch equations (1c)-(1e) are separated in time as described in [23] for the QCL including self-induced transparency and in [5] for the active mode-locking of MIR QCL. The advantage of this method is the easier implementation of Maxwell-Bloch equations using the one-dimensional FDTD method. Thus, the electric field is computed at time steps  $n\Delta t$  while Bloch equations and the magnetic field are computed at time steps  $(n + \frac{1}{2})\Delta t$ . However, a wise choice of time steps is to be considered because it has been demonstrated in [24] that inconsistent time centering of the discretized derivatives results in a more restrictive stability condition than the original FDTD formulation for dispersive media. The discretized Maxwell-Bloch equations in one-dimensional problem become then

$$H_{m+\frac{1}{2}}^{n+\frac{1}{2}} = H_{m+\frac{1}{2}}^{n-\frac{1}{2}} - \frac{\Delta t}{\mu_0 \Delta y} (E_{m+1}^n - E_m^n) \quad (9a)$$

$$E_m^{n+1} = E_m^n - \frac{\Delta t}{\varepsilon \Delta y} \left[ H_{m+\frac{1}{2}}^{n+\frac{1}{2}} - H_{m-\frac{1}{2}}^{n+\frac{1}{2}} \right] - \frac{\Delta t N \mu}{\varepsilon T_2} \rho_{a_m}^{n+\frac{1}{2}} + \frac{\Delta t N \mu \omega_0}{\varepsilon} \rho_{b_m}^{n+\frac{1}{2}} - \Delta t l_0 \frac{E_m^n + E_m^{n+1}}{2} \quad (9b)$$

$$\rho_{a_m}^{n+\frac{1}{2}} = \rho_{a_m}^{n-\frac{1}{2}} - \frac{\Delta t}{2T_2} \left[ \rho_{a_m}^{n+\frac{1}{2}} + \rho_{a_m}^{n-\frac{1}{2}} \right] + \frac{\Delta t \omega_0}{2} \left[ \rho_{b_m}^{n+\frac{1}{2}} + \rho_{b_m}^{n-\frac{1}{2}} \right] \quad (9c)$$

$$\rho_{b_m}^{n+\frac{1}{2}} = \rho_{b_m}^{n-\frac{1}{2}} - \frac{\Delta t \omega_0}{2} \left[ \rho_{a_m}^{n+\frac{1}{2}} + \rho_{a_m}^{n-\frac{1}{2}} \right] - \frac{\Delta t}{2T_2} \left[ \rho_{b_m}^{n+\frac{1}{2}} + \rho_{b_m}^{n-\frac{1}{2}} \right] + \frac{\Delta t \mu E_m^n}{\hbar} \left[ \Delta_m^{n+\frac{1}{2}} + \Delta_m^{n-\frac{1}{2}} \right] \quad (9d)$$

$$\Delta_m^{n+\frac{1}{2}} = \Delta_m^{n-\frac{1}{2}} - \frac{\Delta t \mu E_m^n}{\hbar} \left[ \rho_{b_m}^{n+\frac{1}{2}} + \rho_{b_m}^{n-\frac{1}{2}} \right] - \frac{\Delta t}{2T_1} \left[ \Delta_m^{n+\frac{1}{2}} + \Delta_m^{n-\frac{1}{2}} \right] + \Delta t I + \frac{\Delta t}{\Delta y} D \left[ \Delta_{m+1}^{n-\frac{1}{2}} - 2\Delta_m^{n-\frac{1}{2}} + \Delta_{m-1}^{n-\frac{1}{2}} \right] \quad (9e)$$

where index  $m$  corresponds to spatial locations and index  $n$  to time steps.

### B. Single-layer graphene highly reflective mirror

The highly reflective mirror is composed of the single-layer graphene and a Bragg mirror. This mirror is formed by a succession of high and low refractive index material layers. The thickness of each layer is equal to a quarter wavelength  $\frac{\lambda_q}{4}$  where the sub-index  $q$  refers to the considered material. The Bragg mirror is modeled using Maxwell equations as given by expressions (5a) and (5b) with the conductivity set to zero.

As for the QCL gain medium, the electric field is calculated at time steps  $n\Delta t$  and the magnetic field is determined at time steps  $(n + \frac{1}{2})\Delta t$ . The discretization of Maxwell equations for graphene effective layer is

$$H_{m+\frac{1}{2}}^{n+\frac{1}{2}} = H_{m+\frac{1}{2}}^{n-\frac{1}{2}} - \frac{\Delta t}{\mu_0 \Delta y} (E_m^{n+1} - E_m^n) \quad (10a)$$

$$E_m^{n+1} = \frac{1}{B} \left[ A E_m^n - \frac{\Delta t}{\varepsilon_0 \varepsilon_{rg} \Delta y} \left( H_{m+\frac{1}{2}}^{n+\frac{1}{2}} - H_{m-\frac{1}{2}}^{n+\frac{1}{2}} \right) \right] \quad (10b)$$

where

$$A = 1 - \frac{n}{\varepsilon_M \eta_0} \Delta t \left[ \alpha_{ns} + \alpha_s \left( 1 + \left( \frac{E_m^n + E_m^{n+1}}{2 E_s} \right)^2 \right)^{-1} \right]$$

$$B = 1 + \frac{n}{\varepsilon_M \eta_0} \Delta t \left[ \alpha_{ns} + \alpha_s \left( 1 + \left( \frac{E_m^n + E_m^{n+1}}{2 E_s} \right)^2 \right)^{-1} \right]$$

The expression (10b) cannot be solved directly due to the square term of the electric fields at time steps  $n\Delta t$  and  $(n + 1)\Delta t$ . An additional numerical method is needed to deal with these two equations and the fixed-point method has been chosen. This method consists of an iterative resolution of nonlinear equations by numerical approximation of the root, here the unknown electric field at time step  $(n + 1)\Delta t$ , in the form  $E_m^{n+1} = f(E_m^{n+1})$  [25].

## IV. SIMULATION PARAMETERS

Table I summarizes the physical parameters of graphene [11] and Bragg mirror used in simulations. The Bragg mirror has been built with *PbSe* and *BaF<sub>2</sub>* materials. The QCL parameters are the same as those given in [3], [4] and [5].

TABLE I  
PHYSICAL PARAMETERS USED IN SIMULATION

Parameters	Symbol	Value
Saturation intensity	$I_s \left( \frac{MW}{cm} \right)$	0.2
Saturable loss	$\alpha_s \text{ (m}^{-1}\text{)}$	$2.32 \cdot 10^7$
Non-saturable loss	$\alpha_{ns} \text{ (m}^{-1}\text{)}$	$2.09 \cdot 10^6$
Relative dielectric constant	$\varepsilon_{PbSe}$	5
Relative dielectric constant	$\varepsilon_{BaF_2}$	1.4
Relative dielectric constant	$\varepsilon_{SiO_2}$	1.5

For the highly reflective mirror, the thicknesses of *PbSe* and *BaF<sub>2</sub>* layers are respectively fixed to  $\frac{\lambda_q}{4}$ . The thickness of the *SiO<sub>2</sub>* layer permits to control the overlap of the maximum field intensity with graphene. A field intensity enhancement factor up to 400% has been obtained using such distance from the reflective mirror in [17]. Because of the standing waves establishment due to the incoming and reflected waves at the mirror, the field intensity depends on the distance  $y$  from the mirror location. Thus, the position of the graphene layer is chosen to maximize the interaction between the field intensity and the graphene layer. The initial value of *SiO<sub>2</sub>* is set to  $\frac{\lambda_{SiO_2}}{4}$  and thereafter changed to analyse its effect on the mode-locking stability. The field intensity is shown in Fig. 2 where the point  $y = 0$  represents the graphene location. As it is shown, the field intensity is maximum for a thickness of *SiO<sub>2</sub>* layer equal to  $\frac{\lambda_{SiO_2}}{4}$ .

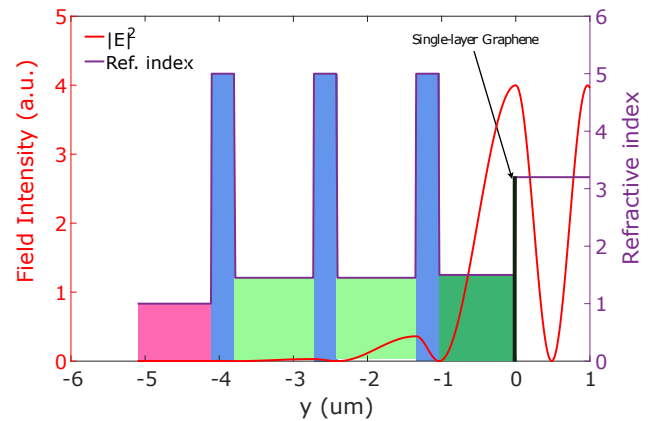


Fig. 2. Normalized field intensity (red curve) and the mirror refractive index profile for  $d_{SiO_2} = \frac{\lambda_{SiO_2}}{4}$ .

## V. OBTAINED RESULTS

We start the analysis with a MIR QCL of a diagonal radiative transition characterized by a relaxation time  $T_1$  around 50 ps which is in the order of the roundtrip time of the laser

cavity. Fig. 3 shows simulation results of the passive mode-locking integrating the single-layer graphene and the highly reflective mirror. We can observe the presence of a single pulse per roundtrip time for the injection pumping rate  $a_p = 1.1$ . The pumping rate is defined as the ratio of the injected current to threshold value.

The pulse is characterized by a peak field intensity of  $12.8 \left[ \frac{MV}{m} \right]$  and a duration of  $56.7 fs$ . This maximum electric field is higher than the field obtained for the active mode-locking with the same structure parameters [5]. This is due to the highly reflective mirror where the light power is totally reflected at this laser facet. The pulse duration is also shortened with the added graphene-based mirror.

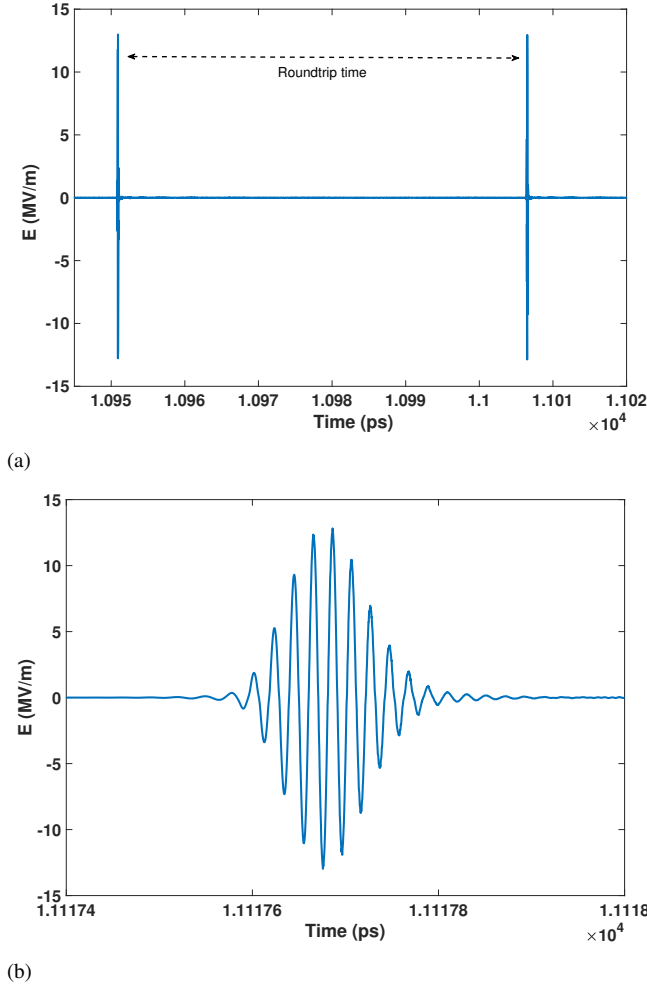


Fig. 3. Time evolution of the electric field for a pumping ratio  $a_p = 1.1$  (a) two pulses and (b) zoom of one pulse.

The increase of pumping rate until 2 maintains the generation of single pulses per roundtrip as is illustrated in Fig. 4.a. The effect of SHB is negligible because the saturable absorber favors the propagation of high intensity pulses and absorbs pulse windings of low intensities. The effect of SHB outweighs the absorption from  $a_p = 3$ . In this case, the intensity of the side peaks of laser pulses becomes strong inducing the apparition of multiple pulses per roundtrip. Fig. 4.b describes the output field for  $a_p = 3$  where 2 pulses per roundtrip are obtained.

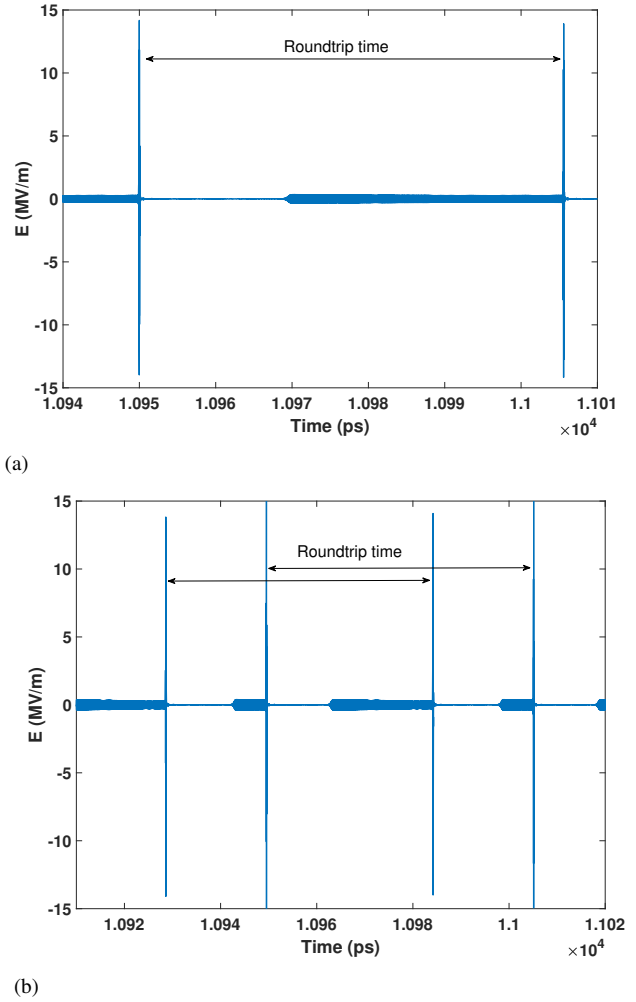


Fig. 4. Time evolution of the electric field for pumping ratio (a)  $a_p = 2$  and (b)  $a_p = 3$

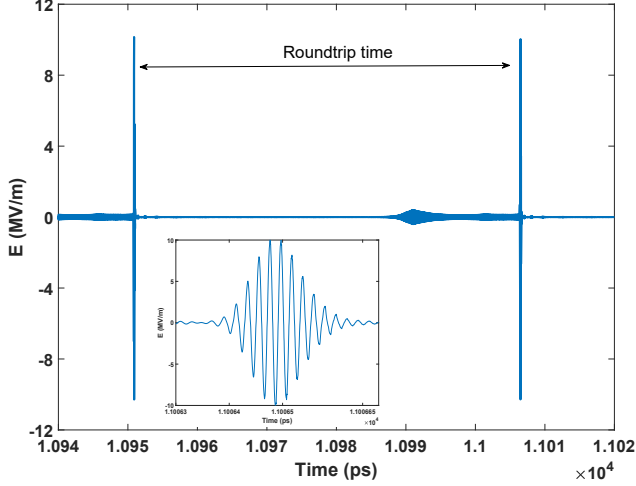
To optimize the structure so that the effect of SHB can be lowered by the absorbing mirror, we move the position of the graphene layer by changing the thickness of  $SiO_2$  layer. In [17], the relation between the absorption of graphene and the thickness of  $SiO_2$  layer was given by the field intensity enhancement factor  $\xi_{ab}$  as following

$$\xi_{ab}(d_{SiO_2}) \approx \frac{4}{1 + n_{SiO_2}^2 \cot^2 \left( \frac{2\pi}{\lambda_{SiO_2}} n_{SiO_2} d_{SiO_2} \right)} \quad (11)$$

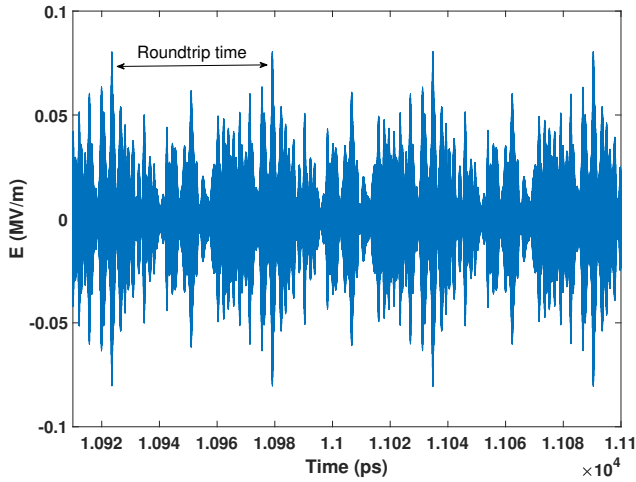
We exploit this expression to determine the position that maximizes this factor. For  $d_{SiO_2} = \frac{\lambda_{SiO_2}}{4}$ , the enhancement factor is  $\xi_{ab} \left( \frac{\lambda_{SiO_2}}{4} \right) = 4$ . This means that the graphene absorption is  $\xi_{ab}(d_{SiO_2}) \times 2.3\% = 9.2\%$ . For  $d_{SiO_2} = \frac{\lambda_{SiO_2}}{8}$ , the absorption is  $\xi_{ab}(d_{SiO_2}) \times 2.3\% = 2.83\%$  while it is close to zero for  $d_{SiO_2} = \frac{\lambda_{SiO_2}}{2}$ .

The simulation with these  $SiO_2$  thicknesses have been done. For the initial thickness  $d_{SiO_2} = \frac{\lambda_{SiO_2}}{4}$ , a stable mode-locking has been obtained with a peak electric field magnitude equal to  $12.8 \left[ \frac{MV}{m} \right]$  (Fig. 3). When the thickness of  $SiO_2$  is decreased to  $\frac{\lambda_{SiO_2}}{8}$ , stable mode-locking remains with a peak electric field decreasing to  $10.26 \left[ \frac{MV}{m} \right]$  and a duration

of 51.8 fs as is shown in Fig. 5.a. Thus, we can observe the dependence of the pulse peak with graphene location. For  $d_{SiO_2} = \frac{\lambda_{SiO_2}}{2}$ , the mode-locking becomes unstable and continuous wave operation governs the laser dynamic. The output field of the QCL is represented in Fig. 5.b which reveals that the graphene layer does not have any effect.



(a)

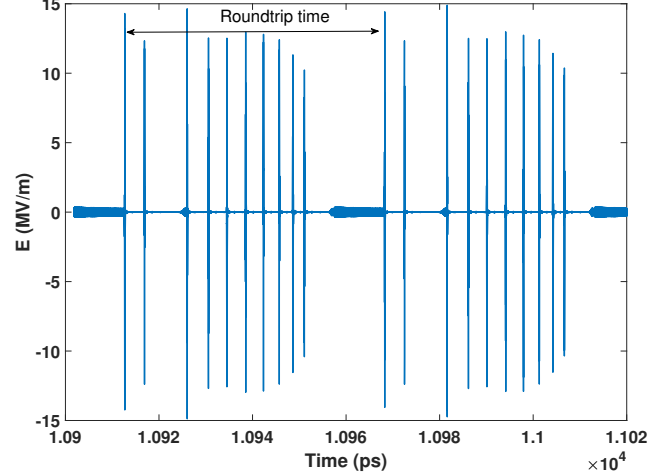


(b)

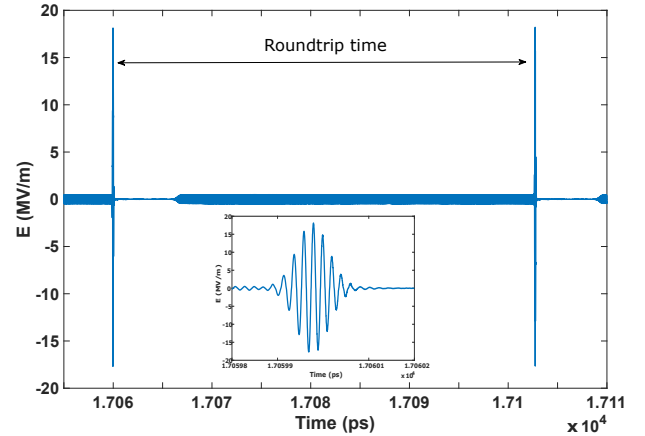
Fig. 5. Time evolution of the electric field for pumping rate  $a_p = 1.1$  and  $d_{SiO_2}$  of (a)  $\frac{\lambda_{SiO_2}}{8}$  and (b)  $\frac{\lambda_{SiO_2}}{2}$ .

We then consider the case of a MIR QCL of a vertical radiative transition that is associated to a shorter relaxation times of 5 ps. Simulation results show that the SHB effect is strong with a short gain recovery time and leads to multiple pulse generation per roundtrip, as highlighted in Fig. 6.a for  $a_p = 1.1$ . The intensity of the generated pulses is greater than the saturation intensity of graphene making its role ineffective. It is evident that the result is more pronounced with shorter relaxation time typically in the range 0.5 – 1 ps for high efficient devices. However, as the SHB effect depends on the induced grating of carrier population it can be controlled through the cavity length. Fig. 6.b shows an improved passive mode-locking once the cavity length is reduced to 1.8 mm. A single pulse per roundtrip is obtained with a peak electric field

of 18  $[\frac{MV}{m}]$  because losses are reduced with a shortened cavity. The pulse duration is slightly lower with a value of 51 fs. However, further simulations have shown that the relaxation time to 1 ps disturbs again the mode-locking stability and shorter cavity length is required for the generation of isolated pulses per roundtrip.



(a)



(b)

Fig. 6. Time evolution of the electric field for pumping rate  $a_p = 1.1$  and  $T_1 = 5$  ps for a cavity length of (a) 2.6 mm and (b) 1.8 mm.

## VI. CONCLUSION

We demonstrate in this paper the passive mode-locking capability of MIR QCLs by incorporating a highly reflective graphene-based mirror. The graphene is used here as a saturable absorber layer and the highly reflective mirror is employed to increase the field intensity in the laser cavity. The overlap between the maximal electric field and graphene layer can be controlled through a thin layer of  $SiO_2$  material. The QCL modeling is performed thanks to the well-known Maxwell-Bloch equations which are solved using FDTD method. The graphene and Bragg grating are modeled with Maxwell's equations according to the nonlinear conductivity of the single-layer graphene related to the intensity-dependent absorption coefficient. The real thickness of the graphene layer

has been simulated without increasing the FDTD simulation time while adapting the FDTD scheme to the presence of this thin sheet.

The QCL structure with a diagonal transition is firstly simulated because the effect of SHB is weaker compared to the QCL structure with a vertical transition. Simulation results with  $T_1 = 50$  ps have shown a stable passive mode-locking when the pumping rate  $a_p$  is less than 3. Beyond this value, a secondary pulse appears and more when the pumping rate increases. However, the location of the graphene layer from the reflective mirror has to be carefully chosen as the graphene layer is more effective when placed at the maximal intensity position. We have shown that an optimized location corresponds to a distance of a quarter wavelength  $\frac{\lambda_{SiO_2}}{4}$  between the Bragg mirror and the graphene layer for which the electric field intensity attains the maximum value. Without graphene, the QCL operates in a continuous waves mode which means mode-locking failure. For a QCL structure with a vertical transition, SHB effect dominates because of the fast recovery time with regard to the cavity roundtrip time. With  $T_1 = 5$  ps, multiple pulses per roundtrip are obtained in 2.6 mm cavity length. However, isolated pulses are obtained by reducing the cavity length to 1.8 mm. Thus, passive mode-locking of the MIR QCL is obtained by integrating a graphene reflective mirror but requires shorter cavity length for  $T_1$  in the range  $0.5 - 1$  ps.

#### REFERENCES

- [1] R.F. Kazarinov and R.A. Suris, "Possibility of the amplification of electromagnetic waves in a semiconductor with a superlattice," *Sov. Phys. Semicond.*, vol. 5, no. 4, pp. 707–709, 1971.
- [2] J. Faist, F. Capasso, D. L. Sivco, C. Sirtori, A. L. Hutchinson, and A. Y. Cho, "Quantum Cascade Laser," *Science* (80), vol. 264, no. 5158, pp. 553–556, Apr. 1994, doi: 10.1126/science.264.5158.553
- [3] C. Y. Wang et al., "Mode-locked pulses from mid-infrared Quantum Cascade Lasers," *Opt. Express*, vol. 17, no. 15, p. 12929, Jul. 2009, doi: 10.1364/OE.17.012929.
- [4] V.-M. Gkortsas et al., "Dynamics of actively mode-locked Quantum Cascade Lasers," *Opt. Express*, vol. 18, no. 13, p. 13616, Jun. 2010, doi: 10.1364/OE.18.013616.
- [5] A. Outafat, S. Faci, E. Richalot, S. Protat and C. Algani, "Active Modelocking Improvement of MIR-QCL by Integrating Graphene as a Saturable Absorber," in *IEEE Journal of Quantum Electronics*, vol. 58, no. 5, pp. 1-8, Oct. 2022, Art no. 2300108, doi: 10.1109/JQE.2022.3177220.
- [6] M. A. Talukder and C. R. Menyuk, "Quantum coherent saturable absorption for mid-infrared ultra-short pulses," *Opt. Express*, vol. 22, no. 13, p. 15608, 2014, doi: 10.1364/oe.22.015608.
- [7] M. A. Talukder and C. R. Menyuk, "Self-induced transparency modelocking of quantum cascade lasers in the presence of saturable nonlinearity and group velocity dispersion," *Opt. Express*, vol. 18, no. 6, p. 5639, Mar. 2010, doi: 10.1364/OE.18.005639.
- [8] R. R. Nair et al., "Fine Structure Constant Defines Visual Transparency of Graphene," *Science* (80-), vol. 320, no. 5881, pp. 1308–1308, Jun. 2008, doi: 10.1126/science.1156965.
- [9] Q. Bao and K. P. Loh, "Graphene photonics, plasmonics, and broadband optoelectronic devices," *ACS Nano*, vol. 6, no. 5, pp. 3677–3694, 2012, doi: 10.1021/nn300989g.
- [10] G. Zhu et al., "Graphene Mode-Locked Fiber Laser at 2.8  $\mu\text{m}$ ," *IEEE Photonics Technol. Lett.*, vol. 28, no. 1, pp. 7–10, Jan. 2016, doi: 10.1109/LPT.2015.2478836.
- [11] A. Mock, "Modeling Passive Mode-Locking via Saturable Absorption in Graphene Using the Finite-Difference Time-Domain Method," *IEEE J. Quantum Electron.*, vol. 53, no. 5, pp. 1–10, Oct. 2017, doi: 10.1109/JQE.2017.2732399.
- [12] F. P. Mezzapesa et al., "Terahertz Frequency Combs Exploiting an On-Chip, Solution-Processed, Graphene-Quantum Cascade Laser Coupled-Cavity," *ACS Photonics*, vol. 7, no. 12, pp. 3489–3498, 2020, doi: 10.1021/acsp Photonics.0c01523.
- [13] Q. Bao et al., "Atomic-Layer Graphene as a Saturable Absorber for Ultrafast Pulsed Lasers," *Adv. Funct. Mater.*, vol. 19, no. 19, pp. 3077–3083, Oct. 2009, doi: 10.1002/adfm.200901007.
- [14] V. Kumar, A. Kumar, D.-J. Lee, and S.-S. Park, "Estimation of Number of Graphene Layers Using Different Methods: A Focused Review," *Materials* (Basel), vol. 14, no. 16, p. 4590, Aug. 2021, doi: 10.3390/ma14164590.
- [15] Xiaohui Li et al., "Broadband Saturable Absorption of Graphene Oxide Thin Film and Its Application in Pulsed Fiber Lasers," *IEEE J. Sel. Top. Quantum Electron.*, vol. 20, no. 5, pp. 441–447, Sep. 2014, doi: 10.1109/JSTQE.2014.2312952.
- [16] J. G. Maloney and G. S. Smith, "The efficient modeling of thin material sheets in the finite-difference time-domain (FDTD) method," *IEEE Trans. Antennas Propag.*, vol. 40, no. 3, pp. 323–330, Mar. 1992, doi: 10.1109/8.135475.
- [17] C. A. Zaugg et al., "Ultrafast and widely tuneable vertical-external-cavity surface-emitting laser, mode-locked by a graphene-integrated distributed Bragg reflector," *Opt. Express*, vol. 21, no. 25, p. 31548, Dec. 2013, doi: 10.1364/OE.21.031548.
- [18] R. W. Ziolkowski, J. M. Arnold, and D. M. Gogny, "Ultrafast pulse interactions with two-level atoms," *Phys. Rev. A*, vol. 52, no. 4, pp. 3082–3094, Oct. 1995, doi: 10.1103/PhysRevA.52.3082.
- [19] S. Singh, A. Tyagi, and B. Vidhani, "Physics of Absorption and Generation of Electromagnetic Radiation", in *Electromagnetic Wave Propagation for Industry and Biomedical Applications*. London, United Kingdom: IntechOpen, 2021.
- [20] F. T. Vasko, "Saturation of interband absorption in graphene," *Phys. Rev. B*, vol. 82, no. 24, p. 245422, Dec. 2010, doi: 10.1103/PhysRevB.82.245422.
- [21] Kane Yee, "Numerical solution of initial boundary value problems involving Maxwell's equations in isotropic media," *IEEE Trans. Antennas Propag.*, vol. 14, no. 3, pp. 302–307, May 1966, doi: 10.1109/TAP.1966.1138693.
- [22] A. Taflov, S. C. Hagness and M. Piket-May, "Computational Electromagnetics: The Finite-Difference Time-Domain Method," in *The Electrical Engineering Handbook*. Elsevier, 2005, pp. 629–670.
- [23] A. Outafat, S. Faci, E. Richalot, S. Protat and C. Algani, "Passive modelocking MIR quantum cascade laser incorporating self-induced transparency," *Opt. Quant. Electron* 54, 283 (2022). doi: 10.1007/s11082-022-03675-y.
- [24] P. G. Petropoulos, "Stability and phase error analysis of FD-TD in dispersive dielectrics," in *IEEE Transactions on Antennas and Propagation*, vol. 42, no. 1, pp. 62–69, Jan. 1994, doi: 10.1109/8.272302.
- [25] E. Djalal, A. Belahcen, and A. Arkkio, "A fast fixed-point method for solving magnetic field problems in media of hysteresis," *IEEE Trans. Magn.*, vol. 44, no. 6, pp. 1214–1217, 2008, doi: 10.1109/TMAG.2007.916673.

**Amine Outafat** received the Ph.D. degree in Photonics from Gustave Eiffel University, France, in 2022 and a Master degree in electronics from Paris-Est Marne-la-Vallée University, France, in 2018. He follows currently a postdoctoral position at Gustave Eiffel university and carry out his research in the Electronic, Communication Systems and Microsystems Laboratory (Esycom). His research topic concerns the numerical modeling of photonic devices and specifically Quantum Cascade Lasers.

**Salim Faci** received the Dipl. Ing. degree in electronics from Mouloud Mammeri University, Tizi-Ouzou, Algeria, in 2001, the M.D. degree in electronics from Sorbone University, Paris, France, in 2003, and the Ph.D. degree in electronics and photonics from Sorbone University, in 2007. His doctoral research focused on photoconductive switches modeling and optical control of microwave oscillators. Since 2011, he is with the Electronic, Communication Systems and Microsystems Laboratory (Esycom Lab.), Paris, France, and his research has focused on microwave photonics which includes RoF systems, photonic generation of mm-wave signals, and optoelectronic devices modeling. His research interests include optical fiber distributed sensors for health structure monitoring and MIR spectroscopy for sensing applications.

**Elodie Richalot** received the Diploma and Ph.D. degrees in electronics engineering from the école Nationale Supérieure d'électrotechnique, d'électronique, d'Informatique, d'Hydraulique Toulouse, Toulouse, France, in 1995 and 1998, respectively. Since 1998, she has been with the University of Paris-Est Marne-la-Vallée, Champs-sur-Marne, France, where she became a Professor in electronics in 2010. Her current research activities in ESYCOM laboratory include modeling techniques, electromagnetic compatibility and reverberation chambers, and millimeter wave passive devices and sensors.

**Stéphane Protat** was born in 1967, France. He received Ph.D. degrees in electrical engineering from Université Paris-Est Marne-la-Vallée, Marne-la-Vallée, France, in 1999. He was a research fellow in modal analysis at ESA/ESTEC, Noordwijk, Netherland in 2001. In 2006, he joined, the Electronic, Communication Systems and Microsystems Laboratory (Esycom), Gustave Eiffel University, Marne-la-vallée, where he is currently research engineer in Electronics. His past and present research interests in FDTD computation, including electromagnetic simulations of antennas, radio frequency identification (RFID) technologies, RFID localization.

**Catherine Algani** received the DEA degree in electronics from the University of Paris 6, Paris, France, in 1987 and the Ph.D. degree in active MMIC design using GaAs HBTs technology from the University of Paris 6, Paris, France, in 1990. In 1991, she joined the Electronics Engineering Department and the LISIF Laboratory, University Pierre et Marie Curie, as an Assistant Professor. She worked on the design of microwave and millimeter-wave integrated circuits and in microwave photonics. In 2005, she joined ESYCOM Laboratory, Le CNAM, Paris, France, where she is currently a Full Professor, working on the development of microwave-photonics devices, circuits, and sub-systems for ROF and wireless applications.